

Superfluid vortex dynamics on a spherical film

Sálvio J. Bereta^{✉*} and Mônica A. Caracanhas[✉]

Instituto de Física de São Carlos, Universidade de São Paulo, São Paulo, Brazil

Alexander L. Fetter^{✉†}

Departments of Physics and Applied Physics, Stanford University, Stanford, California 94305-4045, USA



(Received 22 January 2021; accepted 19 April 2021; published 6 May 2021)

Motivated by ongoing experimental efforts to make closed Bose-Einstein condensate shells in microgravity environments, this work studies the energy and dynamics of singly quantized vortices on a thin spherical superfluid shell, where the overall vortex charge must vanish (as on any compact surface). For each vortex, stereographic projection yields the corresponding complex potential on the tangent plane. The resulting stream function then provides both the total energy and the dynamics of a system of overall neutral vortices on a spherical film. Although a single-vortex dipole follows a simple dynamical orbit, four vortices can present a variety of situations. We study a few symmetric initial configurations and then focus on the special case of two small vortex dipoles.

DOI: [10.1103/PhysRevA.103.053306](https://doi.org/10.1103/PhysRevA.103.053306)

I. INTRODUCTION

The remarkable creation (1995) of Bose-Einstein condensates (BECs) in ultracold dilute atomic gases has renewed interest in bosonic superfluids (see, for example, Refs. [1,2]). These highly flexible many-body coherent systems now appear in many different forms, for example, three-dimensional bulk condensates ranging from flat pancakes to elongated cigars and various optical lattices. They also provide a basis for tests of fundamental quantum matter [3].

Recent proposals to create thin spherical traps in space (leading to “bubble” BECs) [4,5] along with the related works in Refs. [6,7] have stimulated research on thin-film superfluid dynamics on curved surfaces [8,9]. Here we study thin spherical superfluids that we model as ideal classical fluid films with quantized vortices. In addition, the compact spherical surface requires that the system have zero net vorticity.

Several authors have studied the dynamics of classical vortices in incompressible two-dimensional spherical fluids [10–13], mostly focused on geophysical applications. For such classical vortices on a sphere, the topological constraint of vanishing total vorticity is readily satisfied. For example, Ref. [14] includes a detailed study of the dynamics of three classical vortices. In contrast, we study singly quantized superfluid vortices, where three such vortices cannot occur on a sphere. Although other authors have studied quantized point vortices on curved surfaces, they emphasize the energy (see, for example, Ref. [15]), usually based on the phase $S(\mathbf{r})$ of the superfluid condensate wave function. Instead we focus here on the dynamics of these quantized vortices and specialize to the surface of a sphere.

To this end, we rely on the stream function $\chi(\Omega)$ at a point with spherical polar angular coordinates $\Omega = (\theta, \phi)$. In addition, χ also depends parametrically on the location of the various point vortices at Ω_j . Not only does χ determine directly the motion of the set of vortices, but it also immediately gives the interaction energy of the same vortices with no additional analysis. A combination of these results generalizes the familiar Hamiltonian formulation of vortex dynamics on a plane to the curved surface of a sphere, with the angular coordinates of a vortex $\Omega_j = (\theta_j, \phi_j)$ as canonical Hamiltonian variables (see, for example, Sec. 157 of Ref. [10]).

In Sec. II we summarize vortex dynamics in a plane, where we review the complementary roles of the condensate phase S (which is effectively the velocity potential) and of the stream function χ in determining the local flow velocity $\mathbf{v}(\mathbf{r})$. For the surface of a sphere (Sec. III), we use a stereographic projection to determine the corresponding stream function $\chi(\Omega)$ and hence the vortex dynamics on a sphere. As an example, we study the dynamics of a single vortex dipole. Section IV obtains the energy of a set of vortices on a sphere in terms of the same stream function, which then provides a Hamiltonian formalism for the vortex dynamics. Section V studies the dynamics of four vortices in a few simple symmetric configurations. The energy and dynamics of two small vortex dipoles are considered in Sec. VI, and Sec. VII provides a summary and outlook.

II. SUPERFLUID VORTEX DYNAMICS ON A PLANE

Typical superfluids like He-II and atomic BECs have scalar complex order parameters $\Psi = |\Psi|e^{iS}$. The associated superfluid velocity is

$$\mathbf{v} = (\hbar/M)\nabla S, \quad (1)$$

where $2\pi\hbar = h$ is Planck’s constant and M is the relevant atomic mass. Apart from an overall factor, the phase $S(\mathbf{r})$ is

*salvio.bereta@usp.br

†fetter@stanford.edu

the velocity potential. Equation (1) implies that the superfluid velocity field is irrotational with $\nabla \times \mathbf{v} = 0$ except at singular points that represent quantized vortices. Each vortex has quantized circulation

$$\oint_{\mathcal{C}} d\mathbf{l} \cdot \mathbf{v} = \frac{\hbar}{M} \oint_{\mathcal{C}} d\mathbf{l} \cdot \nabla S = \frac{2\pi\hbar}{M} \nu, \quad (2)$$

where ν is the winding number of the phase around the closed contour \mathcal{C} . The fundamental unit of circulation is $2\pi\hbar/M$, which has the dimension of length squared over time, like a diffusivity or a kinematic viscosity.

In many cases, the fluid is also incompressible with $\nabla \cdot \mathbf{v} = 0$. This property allows an alternative representation of the superfluid velocity field

$$\mathbf{v} = (\hbar/M) \hat{\mathbf{n}} \times \nabla \chi, \quad (3)$$

where $\chi(\mathbf{r})$ is the stream function and $\hat{\mathbf{n}}$ is the unit normal vector to the plane. For a single quantized vortex with integer vortex charge q_0 at \mathbf{r}_0 , the vorticity is singular, with

$$\nabla \times \mathbf{v} = \frac{2\pi\hbar}{M} \hat{\mathbf{n}} q_0 \delta^{(2)}(\mathbf{r} - \mathbf{r}_0). \quad (4)$$

It is not hard to show from Eqs. (3) and (4) that the scalar function χ satisfies Poisson's equation

$$\nabla^2 \chi = 2\pi \sum_{j=1}^{N_v} q_j \delta^{(2)}(\mathbf{r} - \mathbf{r}_j), \quad (5)$$

with the N_v vortices at \mathbf{r}_j and charges q_j serving as sources for the stream function. Note the clear analogy to the two-dimensional electrostatic potential arising from a set of two-dimensional point charges. Like the electrostatic potential, the total stream function χ is defined only up to an additive constant that is generally irrelevant.

Equations (1) and (3) together give the following equations for the Cartesian components of the velocity field:

$$\frac{Mv_x}{\hbar} = \frac{\partial S}{\partial x} = -\frac{\partial \chi}{\partial y}, \quad \frac{Mv_y}{\hbar} = \frac{\partial S}{\partial y} = \frac{\partial \chi}{\partial x}. \quad (6)$$

By inspection, we see that χ and S satisfy the Cauchy-Riemann equations and can be linked to form a single analytic function of a complex variable

$$F(z) = \chi + iS, \quad (7)$$

where $z = x + iy$; its real part immediately provides the desired stream function with $\chi = \text{Re } F$. It also follows directly that

$$v_y + iv_x = \frac{\hbar}{M} \frac{dF}{dz} = \frac{\hbar}{M} F'(z). \quad (8)$$

The complex potential for a single vortex with positive charge $q_0 = 1$ at z_0 is

$$F(z) = \ln(z - z_0). \quad (9)$$

Any complex function $Z(z)$, such as $z - z_0$, can be written in polar form, $Z(z) = |Z(z)| \exp[i \arg Z(z)]$; note that

$|Z| = (ZZ^*)^{1/2}$, where Z^* is the complex conjugate. Correspondingly, the logarithm becomes $\ln Z = \ln |Z| + i \arg Z$, and the real part is $\ln |Z| = \frac{1}{2} \ln |Z|^2$.

For a single positive vortex [compare Eq. (9)], the stream function $\chi_0(\mathbf{r}) = \text{Re } F$ is

$$\chi_0(\mathbf{r}) = \frac{1}{2} \ln |z - z_0|^2 = \ln |\mathbf{r} - \mathbf{r}_0|. \quad (10)$$

The resulting superfluid velocity $\mathbf{v}(\mathbf{r})$ follows from Eq. (8):

$$v_y + iv_x = \frac{\hbar}{M} \frac{1}{z - z_0} = \frac{\hbar}{M} \frac{z^* - z_0^*}{|z - z_0|^2}. \quad (11)$$

If the vortex is at the origin ($z_0 = 0$), we readily recover the familiar axisymmetric circulating irrotational flow

$$\mathbf{v}_0(\mathbf{r}) = \frac{\hbar}{Mr} \hat{\boldsymbol{\phi}}, \quad (12)$$

where (r, ϕ) are plane polar coordinates and $\hat{\boldsymbol{\phi}} = \hat{\mathbf{n}} \times \hat{\mathbf{r}}$ is the unit azimuthal vector in the polar direction.

More generally, for a system of N_v vortices at \mathbf{r}_j with vortex charge q_j ($j = 1, \dots, N_v$), the total hydrodynamic flow field $\mathbf{v}(\mathbf{r})$ is the sum of contributions from each vortex. To make this connection more precise, define

$$\chi_j(\mathbf{r}) = \ln |z - z_j| = \ln |\mathbf{r} - \mathbf{r}_j|. \quad (13)$$

We here consider only singly charged vortices with $q_j = \pm 1$, although most of our analysis applies more generally. The total stream function $\chi(\mathbf{r})$ is the linear combination

$$\chi(\mathbf{r}) = \sum_{j=1}^{N_v} q_j \chi_j(\mathbf{r}) \quad (14)$$

giving the total hydrodynamic flow field

$$\mathbf{v}(\mathbf{r}) = \frac{\hbar}{M} \hat{\mathbf{n}} \times \nabla \chi(\mathbf{r}) = \frac{\hbar}{M} \hat{\mathbf{n}} \times \nabla \sum_j q_j \chi_j(\mathbf{r}). \quad (15)$$

In an ideal fluid, a given vortex moves with the local flow velocity at its position, typically arising from all the *other* vortices. In the present context of an unbounded plane, it follows directly that the k th vortex has the velocity

$$\dot{\mathbf{r}}_k = \frac{\hbar}{M} \hat{\mathbf{n}} \times \sum_j' q_j [\nabla \chi_j(\mathbf{r})]_{\mathbf{r} \rightarrow \mathbf{r}_k}, \quad (16)$$

where the primed sum omits the single term $j = k$. For each term of the sum, the j th coordinate is fixed, so that $[\nabla \chi_j(\mathbf{r})]_{\mathbf{r} \rightarrow \mathbf{r}_k} = \nabla_k \chi_j(\mathbf{r}_k)$. Hence we can simplify this result to

$$\dot{\mathbf{r}}_k = \frac{\hbar}{M} \hat{\mathbf{n}} \times \nabla_k \sum_j' q_j \chi_j(\mathbf{r}_k), \quad (17)$$

which now depends only on the coordinates of the vortices since $\chi_j(\mathbf{r}_k) = \ln |\mathbf{r}_k - \mathbf{r}_j| \equiv \chi_{kj}$. In this way, the individual stream functions χ_j determine both the total hydrodynamic superfluid flow through Eq. (15) and the dynamical motion of each vortex through Eq. (17).

The quantity $\nabla_k \chi_j(\mathbf{r}_k) = (\mathbf{r}_k - \mathbf{r}_j)/|\mathbf{r}_k - \mathbf{r}_j|^2$ is odd under the interchange $j \leftrightarrow k$. It follows immediately from Eq. (17)

that

$$\sum_{k=1}^{N_v} q_k \dot{\mathbf{r}}_k = 0, \quad \text{or, equivalently,} \quad \sum_{k=1}^{N_v} q_k \mathbf{r}_k = \text{const.} \quad (18)$$

Hence the combined dynamical motion of the vortices on a plane conserves this vector quantity $\sum_{k=1}^{N_v} q_k \mathbf{r}_k$. This result is well known for two vortices, but its generalization will be useful in Sec. VI.

III. STEREOGRAPHIC PROJECTION FOR VORTICES ON A SPHERE

Most of the previous summary about vortices on a plane applies also to vortices on the surface of a sphere, but there is one important difference. On a plane, a simple closed curve \mathcal{C} divides the plane into an interior and an exterior, with a clear distinction between them. For example, a point in the interior can serve as a local origin that defines a positive sense of rotation for \mathcal{C} . The phase winding around \mathcal{C} is the net vortex charge enclosed by \mathcal{C} , and the resulting lines of constant phase crossing \mathcal{C} can extend unimpeded through the exterior region.

The situation is very different on the surface of a sphere because of the compact topology. In particular, a closed curve \mathcal{C} divides the spherical surface into two regions, but the choice of interior region appears arbitrary. Choose a point in one of the two regions and use it to define the positive sense for \mathcal{C} , with a resulting phase winding number. From the perspective of the other region, however, \mathcal{C} has a negative sense with the negative of the same phase winding number. This symmetry means that any collection of point vortices on the surface of a sphere must have zero total vortex charge. Sections 80 and 160 of Ref. [10] quote this property in treating a vortex dipole on a sphere as the simplest case with zero net vortex charge, using without proof the method of stereographic projection to give the translational velocity of such a vortex dipole. Here we provide a more complete derivation (see also Refs. [11–14]).

Consider a point vortex in a superfluid film on the surface of a sphere of radius R . To determine the velocity field on the sphere, we use a stereographic projection [16] onto a complex plane. Familiar methods from Sec. II provide the velocity field on the complex plane, and the appropriate coordinate transformation then determines the corresponding solution for the sphere.

In the stereographic projection, we consider a tangent plane at the north pole. Each point on the sphere has a one-to-one correspondence with a point on tangent plane, except for the point at the south pole. As seen from Fig. 1, a point on the sphere with spherical polar coordinates (θ, ϕ) has the corresponding complex coordinate on the plane

$$z = \rho e^{i\phi} \quad \text{with} \quad \rho = 2R \tan(\theta/2) \quad (19)$$

and the same azimuthal angle ϕ .

Section II shows that the complex potential $F(z)$ of a vortex dipole with complex coordinates z_{\pm} and charges $q_{\pm} = \pm 1$ is

$$F_{\text{dip}}(z) = \ln(z - z_+) - \ln(z - z_-) = \ln\left(\frac{z - z_+}{z - z_-}\right), \quad (20)$$

where z is on the tangent plane. The stereographic projection in Eq. (19) gives the transformation $z_{\pm} = 2R \tan(\theta_{\pm}/2)e^{i\phi_{\pm}}$,

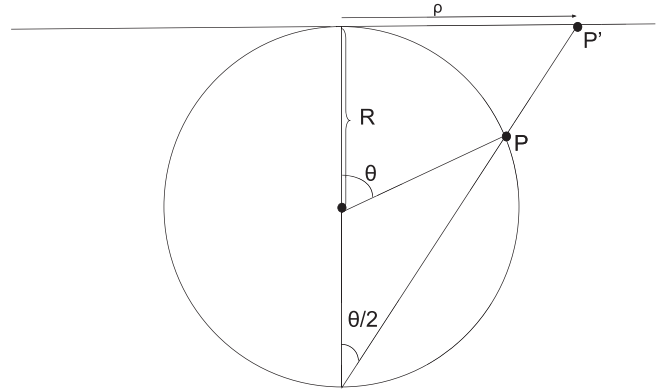


FIG. 1. Stereographic projection of a sphere of radius R onto a tangent plane at the north pole. The figure shows the projection of a generic point P on the sphere to the point P' on the complex plane, with radial distance $\rho = 2R \tan(\theta/2)$ and the same azimuthal angle ϕ .

where $(\theta_{\pm}, \phi_{\pm})$ are the spherical coordinates of the members of the vortex dipole on the sphere, leading to the associated complex function on the sphere

$$F_{\text{dip}} = \ln\left[\frac{\tan(\theta/2)e^{i\phi} - \tan(\theta_+/2)e^{i\phi_+}}{\tan(\theta/2)e^{i\phi} - \tan(\theta_-/2)e^{i\phi_-}}\right], \quad (21)$$

where the overall scale factors $2R$ cancel.

It is helpful to introduce the abbreviation $u = \tan(\theta/2)$ and similarly for u_{\pm} . Application of Eq. (10) for each vortex yields the stream function for a vortex dipole on a sphere

$$\chi_{\text{dip}}(\Omega) = \frac{1}{2} \ln\left[\frac{u^2 + u_+^2 - 2uu_+ \cos(\phi - \phi_+)}{u^2 + u_-^2 - 2uu_- \cos(\phi - \phi_-)}\right], \quad (22)$$

where $\Omega = (\theta, \phi)$ is a convenient notation. Use of the trigonometric identity

$$\tan(\theta/2) = \frac{\sin \theta}{1 + \cos \theta} = \left(\frac{1 - \cos \theta}{1 + \cos \theta}\right)^{1/2} \quad (23)$$

simplifies this result, which can be written as the difference of two separate quantities, each involving a single vortex [compare Eq. (14)]

$$\chi_{\text{dip}}(\Omega) = \chi_+(\Omega) - \chi_-(\Omega). \quad (24)$$

Here [compare Eq. (13)]

$$\chi_j(\Omega) = \frac{1}{2} \ln[2 - 2 \cos \theta \cos \theta_j - 2 \sin \theta \sin \theta_j \cos(\phi - \phi_j)] \quad (25)$$

depends on the variable angular coordinate Ω and the fixed angular coordinate Ω_j of the j th vortex. Note that the factor 2 merely adds a constant term to χ_j and is chosen for convenience. Also, we omit a constant factor $1 + \cos \theta_j$ that depends only on the vortex coordinate and does not affect the fluid velocity. Since Eq. (25) is symmetric in its variables, we can also write it as $\chi_j(\Omega) = \chi(\Omega, \Omega_j)$, which will be useful below.

To interpret Eq. (25), recall the unit radial vector $\hat{\mathbf{r}} = \sin \theta \cos \phi \hat{\mathbf{x}} + \sin \theta \sin \phi \hat{\mathbf{y}} + \cos \theta \hat{\mathbf{z}}$. The dot product with

the corresponding \hat{r}_j for the j th vortex is

$$\hat{r} \cdot \hat{r}_j = \cos \gamma_j = \sin \theta \sin \theta_j \cos(\phi - \phi_j) + \cos \theta \cos \theta_j, \quad (26)$$

where γ_j is the angle between the two vectors. Evidently, Eq. (25) has the equivalent and simpler form

$$\begin{aligned} \chi_j(\Omega) &= \chi(\Omega, \Omega_j) = \frac{1}{2} \ln(2 - 2 \cos \gamma_j) = \ln |\hat{r} - \hat{r}_j| \\ &= \frac{1}{2} \ln[4 \sin^2(\gamma_j/2)] = \ln[2 \sin(|\gamma_j|/2)], \end{aligned} \quad (27)$$

where the square root requires the absolute value $|\gamma_j|$ [compare Eq. (13) for the stream function of a vortex on a plane].

Equation (27) has a simple geometric interpretation. Figure 1 shows that $2R \sin(\theta/2)$ is the chordal distance between the point P and the north pole. Hence $2R \sin(|\gamma_j|/2)$ is the chordal distance between \hat{r} and \hat{r}_j , which is less than the corresponding great-circle distance between them. Note also that $\ln |\hat{r} - \hat{r}_j| = \ln |\mathbf{r} - \mathbf{r}'|/R$. In the limit $R \rightarrow \infty$ for fixed $|\mathbf{r} - \mathbf{r}'|$, Eq. (27) reduces to Eq. (13) for the plane, apart from the irrelevant constant $\ln R$.

For a general set of N_v point vortices with $\sum_j q_j = 0$, the corresponding total stream function is

$$\chi(\Omega) = \sum_j q_j \chi(\Omega, \Omega_j), \quad (28)$$

which depends on the variable observation location Ω and the given locations of all the vortices Ω_j . The total hydrodynamic velocity field is

$$\mathbf{v}(\Omega) = \frac{\hbar}{M} \hat{r} \times \nabla \chi(\Omega) = \frac{\hbar}{M} \hat{r} \times \sum_j q_j \nabla \chi(\Omega, \Omega_j), \quad (29)$$

where \hat{r} is the unit normal vector to the surface of the sphere. Note that the operator $\hat{r} \times \nabla$ is effectively the angular momentum operator and involves only the angular parts of the gradient operator. To be very specific,

$$\hat{r} \times \nabla = -\frac{\hat{\theta}}{R \sin \theta} \frac{\partial}{\partial \phi} + \frac{\hat{\phi}}{R} \frac{\partial}{\partial \theta}, \quad (30)$$

where $(\hat{\theta}, \hat{\phi}, \hat{r})$ form an orthonormal triad on the surface of the sphere, analogous to $(\hat{x}, \hat{y}, \hat{z})$ on the plane.

Just as for a plane, a given vortex on a spherical surface moves with the local velocity generated by all the other vortices [see Eq. (16)]. The argument leading to Eq. (17) readily yields

$$\dot{\mathbf{r}}_k = \frac{\hbar}{M} \hat{r}_k \times \nabla_k \sum_j' q_j \chi(\Omega_k, \Omega_j). \quad (31)$$

The dynamics of the k th vortex now depends only on the angular coordinates of the N_v vortices through the single sum of stream functions

$$\sum_j' q_j \chi(\Omega_k, \Omega_j) = \sum_j' q_j \ln [2 \sin(|\gamma_{kj}|/2)], \quad (32)$$

where $\cos \gamma_{kj} = \hat{r}_k \cdot \hat{r}_j$.

A single-vortex dipole provides a simple example of vortex dynamics on a sphere. The rotational symmetry allows us to place the two vortices at the same azimuth angle $\phi_+ = \phi_-$,

with θ_+ in the upper hemisphere and θ_- in the lower hemisphere (we eventually choose them to be symmetrical around the equator, but we first need to differentiate the stream function with respect to one polar angle, keeping the other polar angle fixed). Equation (27) gives the relevant stream function

$$\chi(\Omega_+, \Omega_-) = \ln \left[2 \sin \left(\frac{\theta_- - \theta_+}{2} \right) \right]. \quad (33)$$

Use of Eq. (31) gives (compare Sec. 160 of Ref. [10])

$$\dot{\mathbf{r}}_+ = \dot{\mathbf{r}}_- = \frac{\hbar}{2MR} \cot \left(\frac{\theta_- - \theta_+}{2} \right) \hat{\phi} = \frac{\hbar}{2MR} \tan \theta \hat{\phi}, \quad (34)$$

where we set $\theta_+ = \theta$ and $\theta_- = \pi - \theta$ after applying the gradient operator. Each member of the vortex dipole moves uniformly in the positive $\hat{\phi}$ direction with fixed separation and speed $v_{\text{dip}} = \hbar \tan \theta / (2MR)$. For small $\theta \ll 1$, the dipole is near the poles and the motion is slow. If the pair is near the equator, however, we have $\theta = \pi/2 - \Delta\theta$ with $\Delta\theta \ll 1$, and $v_{\text{dip}} = \hbar \cot \Delta\theta / (2MR) \approx \hbar / (2MR \Delta\theta)$. This result agrees with the corresponding planar dipole because $2R \Delta\theta$ is the linear separation between the two members of the dipole.

IV. ENERGY OF VORTICES ON A SPHERE

In the present hydrodynamic model, the total energy is simply the kinetic energy $E = \frac{1}{2} M n \int d^2 r |\mathbf{v}(\mathbf{r})|^2$, where n is the two-dimensional uniform number density and the logarithmic divergence near the center of each vortex must be cut off at some small vortex core radius ξ . This picture applies equally to a plane and to the surface of a sphere. A combination with Eq. (29) leads to

$$E = \frac{\hbar^2 n}{2M} \sum_{i,j=1}^{N_v} q_i q_j \int d^2 r \nabla \chi_i \cdot \nabla \chi_j = \frac{\hbar^2 n}{2M} \sum_{i,j=1}^{N_v} q_i q_j I_{ij}, \quad (35)$$

which defines the dimensionless integrals $I_{ij} = \int d^2 r \nabla \chi_i \cdot \nabla \chi_j$. The sum includes both the diagonal terms with $i = j$ and the off-diagonal terms with $i \neq j$.

It is convenient to use the vector identity

$$\nabla A \cdot \nabla B = \nabla \cdot (A \nabla B) - A \nabla^2 B, \quad (36)$$

where A and B are scalar functions. Consider first the diagonal terms, with $A = B = \chi_i$, and exclude a small circle of radius ξ around \mathbf{r}_i , where the relative angle γ_i is small and constant. Since the singularity is excluded, the second term in Eq. (36) vanishes identically, and the first term becomes a line integral around the excluded circular region with radius ξ . In this vicinity, let $\mathbf{s} = \mathbf{r} - \mathbf{r}_i$, and Eq. (27) then shows that $\chi_i \approx \ln s/R$, where R is the radius of the sphere. A detailed analysis readily gives $I_{ii} = 2\pi \ln(R/\xi)$. Note that the resulting self-energy $E_{\text{self}} = (\pi \hbar^2 n/M) \ln(R/\xi)$ is independent of position and the same for all vortices.

For the off-diagonal integrals with $i \neq j$, the above vector identity (36) and Eq. (5) immediately gives the result $I_{ij} = -2\pi \chi_{ij}$, where we use the simplified notation $\chi_{ij} = \chi(\Omega_i, \Omega_j)$. We can now combine our results to find the total

energy

$$E = \frac{\hbar^2 n \pi}{M} N_v \ln \left(\frac{R}{\xi} \right) - \frac{\hbar^2 n \pi}{M} \sum'_{i,j} q_i q_j \chi_{ij}, \quad (37)$$

where the primed double sum omits terms with $i = j$. The first term (the total self-energy of the N_v individual vortices) is an irrelevant additive constant, whereas the second term (the interaction energy) depends explicitly on the position and sign of all the vortices because $\chi_{ij} = \frac{1}{2} \ln [4 \sin^2(\gamma_{ij}/2)]$ involves the relative angle γ_{ij} between the two vortices.

A combination with Eq. (31) leads to the important result

$$\begin{aligned} 2\pi \hbar n q_k \dot{\mathbf{r}}_k &= \frac{2\pi \hbar^2 n}{M} \hat{\mathbf{r}}_k \times \nabla_k \sum'_j q_k q_j \chi(\Omega_k, \Omega_j) \\ &= -\hat{\mathbf{r}}_k \times \nabla_k E, \end{aligned} \quad (38)$$

where we note that

$$\nabla_k \sum'_{i,j} q_i q_j \chi(\Omega_i, \Omega_j) = 2 \nabla_k \sum'_j q_k q_j \chi(\Omega_k, \Omega_j).$$

Also, the total self-energy is constant and hence does not contribute to the induced velocity. The quantity $-\nabla_k E$ can be considered a force on the k th vortex. The hydrodynamics of ideal fluids then ensures that the vortex moves perpendicular to this force, in contrast to the usual Newtonian situation for point masses.

Although Eq. (38) is correct and instructive as written, it can be helpful to separate it into spherical polar components on the sphere's surface. The velocity vector on the surface has the corresponding components

$$\dot{\mathbf{r}} = R \dot{\theta} \hat{\boldsymbol{\theta}} + R \sin \theta \dot{\phi} \hat{\boldsymbol{\phi}}. \quad (39)$$

Also,

$$\nabla_k E = \frac{1}{R} \frac{\partial E}{\partial \theta_k} \hat{\boldsymbol{\theta}}_k + \frac{1}{R \sin \theta_k} \frac{\partial E}{\partial \phi_k} \hat{\boldsymbol{\phi}}_k. \quad (40)$$

A straightforward comparison of terms shows that Eq. (38) has the equivalent form

$$2\pi \hbar n q_k R \dot{\theta}_k = \frac{1}{R \sin \theta_k} \frac{\partial E}{\partial \phi_k}, \quad (41)$$

$$2\pi \hbar n q_k R \sin \theta_k \dot{\phi}_k = -\frac{1}{R} \frac{\partial E}{\partial \theta_k}. \quad (42)$$

As noted by Kirchhoff for point vortices on a plane (see Ref. [10], Sec. 157, and Refs. [11–14]), these equations have a Hamiltonian structure with N_v pairs of conjugate canonical variables (θ_k, ϕ_k) . For singly quantized vortices on a sphere, N_v must be even with $\sum_k q_k = 0$. In the present case, the polar motion $\dot{\theta}_k$ depends on $\partial E / \partial \phi_k$, and similarly the azimuthal motion $\dot{\phi}_k$ depends on $-\partial E / \partial \theta_k$, as seen for a single vortex dipole in Eq. (34).

V. DYNAMICS OF FOUR VORTICES ARRANGED SYMMETRICALLY

In Sec. III we determined the velocity field of a single vortex dipole on a sphere. Equation (34) shows that the dipole moves at constant angular separation parallel to the great circle bisecting them in the direction of the fluid flow between

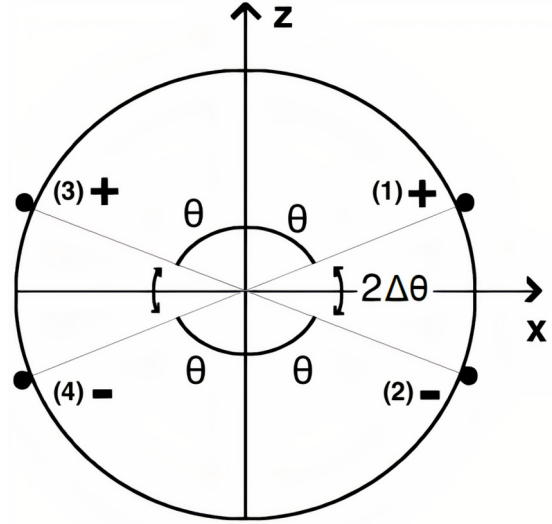


FIG. 2. Coplanar symmetric configuration for four vortices numbered 1 to 4 and charged as shown. We choose initial azimuthal angles $\phi = 0$ (vortices 1 and 2) and $\phi = \pi$ (vortices 3 and 4) and initial polar angles θ (vortices 1 and 3) and $\pi - \theta$ (vortices 2 and 4) measured from the z axis. The figure shows the angular aperture $2\Delta\theta = \pi - 2\theta$ for vortex dipoles (12) and (34), where $\Delta\theta = \pi/2 - \theta$.

them. The speed of the dipole depends only on the cotangent of the half the angular aperture between them.

Some simple configurations of four vortices

The next simplest case is four vortices with overall charge neutrality. Among many initial configurations, some have particularly simple dynamical trajectories. Here we explore two coplanar initial configurations (symmetric and antisymmetric or exchanged) along with the three-dimensional tetrahedral configuration.

1. Symmetric configuration ++ --

Figure 2 illustrates what we call the symmetric coplanar vortex configuration, where we choose the coordinate axes with all four vortices initially in the xz plane. Vortices 1 (positive) and 2 (negative) have the same azimuthal coordinates $\phi_{1,2} = 0$, and symmetric polar coordinates $\theta_1 = \theta$ and $\theta_2 = \pi - \theta$ around the equator. The other two vortices 3 (positive) and 4 (negative) are mirror images of vortices 1 and 2, respectively, reflected in the yz plane, with polar angles $\theta_3 = \theta$ and $\theta_4 = \pi - \theta$, and azimuthal coordinates $\phi_{3,4} = \pi$.

These four vortices behave intuitively in two simple limits: When the vortices are near the poles ($\theta \ll 1$), the two positive (negative) vortices circle the north (south) pole, acting like independent pairs of same-sign vortices, with a linear speed $\hbar / (2MR\theta)$, just like two same-sign vortices on a plane. Near the equator ($\theta \rightarrow \pi/2$ with $\Delta\theta = \pi/2 - \theta \ll 1$) vortices (1,2) and (3,4) act like two independent vortex dipoles and move uniformly with speed $\hbar / (2MR\Delta\theta)$, straddling the equator. For intermediate configurations, all four vortices influence each other, requiring a more detailed analysis.

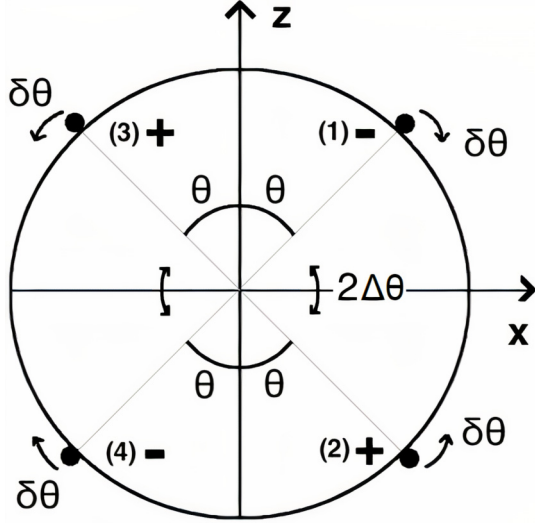


FIG. 3. Coplanar exchanged (antisymmetric) configuration for $\theta = \pi/4$, including the small deviations $\delta\theta$ that provide the orbital motion around the equilibrium position.

Use of Eq. (31) shows that

$$\dot{\mathbf{r}}_k = \sum_{j \neq k} \frac{\hbar}{4MR} \frac{q_j}{\sin^2(\gamma_{kj}/2)} \{-[\sin \theta_j \sin(\phi_k - \phi_j)] \hat{\boldsymbol{\theta}}_k + [\sin \theta_k \cos \theta_j - \cos \theta_k \sin \theta_j \cos(\phi_k - \phi_j)] \hat{\boldsymbol{\phi}}_k\}. \quad (43)$$

For each $k = 1, \dots, 4$, a detailed analysis yields the simple result

$$\dot{\mathbf{r}}_k = \frac{\hbar}{MR} \frac{1}{\sin 2\theta} \hat{\boldsymbol{\phi}}_k = \frac{\hbar}{MR} \frac{1}{\sin 2\Delta\theta} \hat{\boldsymbol{\phi}}_k, \quad (44)$$

where $\Delta\theta = \pi/2 - \theta$. Since these four translational velocities are equal and in the positive azimuthal direction, the vortices all rotate together in a positive (counterclockwise) sense around $\hat{\mathbf{z}}$, remaining coplanar. In appropriate limits, Eq. (44) confirms our previous qualitative discussion.

2. Exchanged (antisymmetric) configuration + - + -

Consider now a second coplanar case, the exchanged configuration, where we interchange the charge of the vortices 1 and 2 in Fig. 2, with $q_1 = -1$ and $q_2 = +1$, as shown in Fig. 3.

For simplicity, we start with $\theta = \theta_0 \ll 1$, when the motion is intuitively clear. Vortices (13) form a vortex dipole near the north pole, with vortices (24) similarly forming a vortex dipole near the south pole. Both dipoles move in the yz plane at fixed $\phi = \pi/2$ toward the equator, where they interact and exchange partners. Vortices (12) then move westward as a dipole along the equator, while vortices (34) similarly move eastward, meeting on the opposite side of the sphere. They then exchange partners again and move toward the north (south) poles, respectively, where the cycle repeats. Note that the positive (negative) vortices execute a close path in the positive (negative) sense relative to the outward normal to the surface of the sphere (a video of the complete simulation is available in the Supplemental Material [17]).

As discussed below Eq. (34), each vortex moves with speed $\hbar/(2MR\theta_0)$ and travels a distance $2\pi R$ in one complete cycle.

Hence the period is $T = 4\pi MR^2\theta_0/\hbar$ and the corresponding angular frequency is

$$\omega = \frac{2\pi}{T} = \frac{\hbar}{2MR^2\theta_0}. \quad (45)$$

Alternatively, we could have started with $\Delta\theta \ll 1$ (see Fig. 3), which executes the same cycle with a different initial position.

The other simple initial configuration is $\theta = \pi/4$ (see Fig. 3). The sign exchange in the summed terms of Eq. (43) means that the velocities $\dot{\mathbf{r}}_k$ all vanish, yielding a static configuration of the four vortices. For small deviations of the initial positions with $\theta = \pi/4 + \delta\theta$, numerical studies (see the Supplemental Material [17]) show that each vortex executes a closed elliptical orbit around its equilibrium static configuration, with positive vortices moving in the positive sense and the negative ones in the negative sense, similar to the motion for the initial configuration $\theta_0 \ll 1$. For $\delta\theta \ll 1$, the elliptical orbit has semiminor and semimajor axes $\approx 2R\delta\theta$ and $\approx 4R\delta\theta$ along $\hat{\boldsymbol{\theta}}$ and $\hat{\boldsymbol{\phi}}$ directions, respectively. Using the numerical data for various values of $\delta\theta$, we found that the analytical formula

$$\omega \approx \frac{\hbar}{MR^2} \frac{1}{\cos(2\delta\theta)} \quad (46)$$

provides a best fit to the numerical values of orbital frequency. For small $\delta\theta$, this frequency reduces to $\omega \approx \hbar/(MR^2)$, whereas for small $\theta \ll 1$ and $\delta\theta \rightarrow -\pi/4$, Eq. (46) gives $\omega \approx \hbar/(2MR^2\theta)$, as expected for the orbital frequency of the dipoles in Eq. (45). The expression in Eq. (46) may well be exact, but we have not found a detailed proof.

For more general asymmetric θ configurations of the four vortices, they will rapidly lose their initial coplanar condition, and we are unable to predict their orbits analytically.

Finally we briefly discuss a three-dimensional tetrahedral configuration, with the vortices at four symmetric sites on the sphere. In contrast to four coplanar vortices, the tetrahedron has only one possible configuration: each positive site will have one positive neighbor and two negative neighbors, all at the same separations. Equation (43) shows that the tetrahedron is also a static vortex configuration. Unlike the planar configurations, however, it is an unstable equilibrium, with complicated dynamics even for small perturbations.

VI. ENERGY AND DYNAMICS OF TWO VORTEX DIPOLES

Section IV considered the energy of a general neutral system of vortices on the surface of a sphere, as given in Eq. (37). The next Sec. V then studied the dynamics of four vortices with zero net vortex charge in some simple symmetric configurations. Here we examine the case of two small vortex dipoles, which is a different special configuration of four vortices with zero net vortex charge. For definiteness, we consider one dipole with charges $q_1 = -q_2 = 1$ and another dipole with $q_3 = -q_4 = 1$. Although Eq. (37) gives the total interaction energy of these two dipoles as a sum over six pairs of vortices, we instead provide a more physical picture.

As a first step, we focus on the small dipole with vortices at angular positions Ω_1 and Ω_2 on the sphere. The total stream

function is

$$\chi^{12}(\Omega) = \chi(\Omega, \Omega_1) - \chi(\Omega, \Omega_2), \quad (47)$$

where Eq. (25) gives the stream function for each individual vortex. For the present case of a small vortex dipole centered at Ω_0 , we write $\delta\Omega_0 = (\delta\theta_0, \delta\phi_0) = \Omega_1 - \Omega_2$ and expand Eq. (47) to first order in the small angular separations. Define the vortex dipole moment (a vector)

$$\mathbf{p}_0 = R\delta\theta_0 \hat{\boldsymbol{\theta}}_0 + R \sin \theta_0 \delta\phi_0 \hat{\boldsymbol{\phi}}_0, \quad (48)$$

which has the dimension of a length, with $\hat{\boldsymbol{\theta}}_0$ and $\hat{\boldsymbol{\phi}}_0$ the unit spherical-polar vectors at Ω_0 on the surface of the sphere. It is not difficult to find

$$\chi_{\text{dip}}(\Omega) \approx -\frac{\mathbf{p}_0 \cdot R(\hat{\mathbf{r}} - \hat{\mathbf{r}}_0)}{R^2(\hat{\mathbf{r}} - \hat{\mathbf{r}}_0)^2} = -\frac{\mathbf{p}_0 \cdot (\mathbf{r} - \mathbf{r}_0)}{(\mathbf{r} - \mathbf{r}_0)^2}, \quad (49)$$

where $\mathbf{r} = R\hat{\mathbf{r}}$ is the coordinate vector normal to the surface of the sphere and we note that $\mathbf{p}_0 \cdot \hat{\mathbf{r}}_0 = 0$. This expression is completely analogous to the electrostatic potential arising from an electric dipole moment \mathbf{p} , here suitably modified for the two-dimensional character of a vortex dipole.

The interaction energy of this single-vortex dipole follows directly from Eq. (37) and the subsequent discussion

$$E_{12} = \frac{2\hbar^2 n\pi}{M} \chi_{12} = \frac{2\hbar^2 n\pi}{M} \ln \left[2 \sin \left(\frac{|\gamma_{12}|}{2} \right) \right]. \quad (50)$$

For a small dipole with $|\gamma_{12}| \ll 1$, we find the simple expression

$$E_{12} \approx \frac{2\hbar^2 n\pi}{M} \ln(|\gamma_{12}|) = -\frac{2\hbar^2 n\pi}{M} \ln \left(\frac{R}{p_{12}} \right), \quad (51)$$

where $p_{12} = R|\gamma_{12}|$ is the separation between the two vortices (it is also the dipole moment). As a result, the energy of the two separate dipoles is

$$E_d = \frac{2\hbar^2 n\pi}{M} (\chi_{12} + \chi_{34}). \quad (52)$$

The interaction energy of the two dipoles is $E_{\text{dd}} = Mn \int d^2r \mathbf{v}^{12} \cdot \mathbf{v}^{34}$, where \mathbf{v}^{12} and \mathbf{v}^{34} are the velocity fields of the two dipoles. Formally, we can use Eqs. (37) and (47) to write

$$\begin{aligned} E_{\text{dd}} &= \frac{\hbar^2 n}{M} \int d^2r \nabla \chi^{34} \cdot \nabla \chi^{12} \\ &= \frac{\hbar^2 n}{M} \int d^2r \nabla(\chi_3 - \chi_4) \cdot \nabla(\chi_1 - \chi_2) \\ &= -\frac{2\pi \hbar^2 n}{M} (\chi_{13} + \chi_{24} - \chi_{23} - \chi_{14}). \end{aligned} \quad (53)$$

The sum of Eqs. (52) and (53) precisely reproduces the six terms inferred from Eq. (37).

More physically, we can find χ^{12} and χ^{34} directly from Eq. (49). In this way, the familiar integration by parts with the first line of Eq. (53) gives an explicit expression for the interaction energy of two small vortex dipoles \mathbf{p} and \mathbf{p}' at positions \mathbf{r} and \mathbf{r}' :

$$E_{\text{dd}} = \frac{2\pi \hbar^2 n}{M} \frac{(\mathbf{p} \cdot \mathbf{p}')(\mathbf{r} - \mathbf{r}')^2 - 2\mathbf{p} \cdot (\mathbf{r} - \mathbf{r}') \mathbf{p}' \cdot (\mathbf{r} - \mathbf{r}')}{(\mathbf{r} - \mathbf{r}')^4}. \quad (54)$$

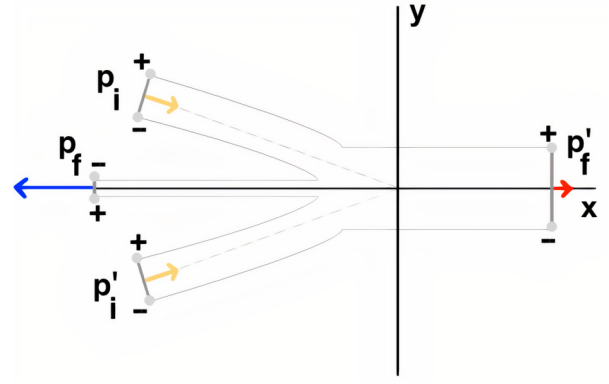


FIG. 4. Two vortex dipoles \mathbf{p}_i and \mathbf{p}'_i move to the right on nearly parallel converging trajectories. Once they are sufficiently close, the individual vortices rearrange to form two new vortex dipoles, with \mathbf{p}_f moving rapidly to the left and \mathbf{p}'_f moving slowly to the right. The solid lines show calculated orbits for the initial conditions.

This rather complicated form is familiar from electrostatics and magnetostatics, suitably modified for the two dimensions relevant here. It varies inversely with the squared separation of the dipoles and is highly anisotropic through the dependence on each dipole's orientation.

We emphasize that Eq. (54) applies only for large separations $|\mathbf{r} - \mathbf{r}'|^2 \gg pp'$ and does not hold for two nearby dipoles. In such a case, we must rely on the general expression from Eq. (37), involving a sum over all six distinct pairs of vortices.

It is interesting to consider the dynamics of two small vortex dipoles on a sphere, say, \mathbf{p}_i and \mathbf{p}'_i . When the two dipoles are well separated, the total energy is the sum of their individual dipole energies $E_{\text{tot}} = -(\pi \hbar^2 n/M) \ln(R^2/p_i p'_i)$, and the magnitudes p_i and p'_i remain fixed as each moves along a great circle at speed $\hbar/M p_i$ and $\hbar/M p'_i$, respectively.

If they approach each other, the dynamics becomes complicated, requiring a detailed analysis. Nevertheless, some general conclusions are possible. For two small nearby dipoles, they interact locally on the tangent plane. We can then invoke the conservation law from Eq. (18), which now implies that the total dipole moment is conserved along with the total energy. In an obvious notation for initial and final dipole moments, we have $\mathbf{p}_i + \mathbf{p}'_i = \mathbf{p}_f + \mathbf{p}'_f$ and the conservation of energy implies that $p_i p'_i = p_f p'_f$.

We already discussed a specific example of two dipoles on a sphere in connection with Fig. 4, when one dipole starts at the north pole and the other starts at the south pole as shown for small dipoles with $\theta \ll 1$. Here we assume that $p'_i = p_i = 2R\theta$. After the interaction, the reconstructed dipoles move around the equator in opposite directions, and the conservation laws then show that $p_f = p'_f = 2R\theta$ during this part of their orbits.

A more unusual situation arises for two nearly parallel dipoles that gradually approach each other (see Fig. 4) in the tangent plane, labeled by axes x and y . Here the initial dipole moments are $\mathbf{p}_i \approx \mathbf{p}'_i \approx p\hat{\mathbf{y}}$, and their motion is principally along $\hat{\mathbf{x}}$ (converging slowly toward the x axis), with each having a small velocity component along $\hat{\mathbf{y}}$. After the interaction, the two inner vortices form a new smaller dipole $\mathbf{p}_f = -p_f \hat{\mathbf{y}}$ that moves to the left. In contrast, the two outer vortices form a

new larger dipole $\mathbf{p}'_f = p'_f \hat{\mathbf{y}}$ that continues moving to the right. The conservation of dipole moment requires $2p = p'_f - p_f$, and the conservation of energy shows that $p^2 = p_f p'_f$. Simple algebra yields the final values $p'_f/p = \sqrt{2} + 1$ and $p_f/p = \sqrt{2} - 1$. As a result, we have a very asymmetric configuration with $p'_f/p_f = 3 + 2\sqrt{2} \approx 5.83$. These two new dipoles move in opposite directions around a single great circle at different speeds, with $v_f/v'_f = 3 + 2\sqrt{2} \approx 5.83$, but they eventually meet. After interacting a second time, they separate and move on nearby great circles toward their initial configuration (see the Supplemental Material [17] for a video of the early evolution of two colliding dipoles).

VII. SUMMARY AND OUTLOOK

We presented the dynamics and stability of singly charged vortices in a thin spherical “bubble” BEC. The compact topology of this system requires an even number of such vortices with total charge zero. We calculated the velocity fields and energies of various configurations of vortices and dipoles, which allow us to determine their dynamics on the surface of the sphere. In some cases, two initial small vortex dipoles can interact and exchange partners. The final reconfigured dipoles then separate and follow new trajectories.

Concerning possible experimental implementation of our model, we assume a thin spherical shell with a superfluid film thickness at most comparable with the vortex core size to avoid vortex-line bending. We also assume near-zero temperature with no dissipation, as appropriate for current experiments on superfluid vortex dynamics [18–20].

As noted in Ref. [21], however, the energy cost for a vortex dipole in this shell geometry will be much lower than for a fully filled spherical condensate of similar size. Thus, we should expect spontaneous nucleation of vortex dipoles at finite temperatures. Although the BEC community generally accepts the GP description of the low-temperature behavior of ultracold dilute atomic gases, the study of the corresponding finite-temperature effects has produced no consensus among the various approaches (see, for example, Ref. [22] for an overview of the principal theoretical techniques). This chal-

lenging topic is not part of our current study and definitely merits future study.

A recent experiment in an earth-orbiting microgravity research laboratory produced a trapped BEC [23], which is a first step toward constructing a “bubble” trap potential. Many theoretical papers have investigated various aspects of a BEC trapped in a spherically symmetric shell potential [6,7,24–26]. In this context, it is important to note that the actual experiment produced an axisymmetric elliptical condensate (a spheroid) using radiofrequency-dressed adiabatic potentials [5,27].

How does the change from a spherical shell to a spheroidal one affect the dynamics of a vortex dipole? To consider this question, recall that a spherical surface has constant Gaussian curvature K , whereas a spheroidal one has a nonuniform K . This situation is analogous to the transition from a cylinder (with vanishing Gaussian curvature) to a torus, where K varies around the surface. On both a sphere and a cylinder [8], a vortex dipole moves uniformly with fixed separation. On a torus, however, a vortex dipole can have many different types of trajectories, depending on the initial position of the vortex dipole (see, for example, Fig. 4 of Ref. [28]). We anticipate that a vortex dipole on a spheroid will exhibit similar behavior and are now studying this very interesting problem.

As an additional complication, we note that Ref. [29] predicted a nonuniform density in a BEC cloud in a spheroidal shell under microgravity, which will affect the vortex dynamics on such a shell. Finally, recent experiments have explored various aspects of superfluid dynamics in the “bubble” trap potential in the presence of gravity and rotation [30,31]. These important unresolved questions exceed the scope of our current study and must remain for future investigation.

ACKNOWLEDGMENTS

We are grateful to Pietro Massignan for helpful discussions and to Vanderlei S. Bagnato for insightful comments. This work was supported by the São Paulo Research Foundation (FAPESP) under Grant No. 2013/07276-1. The authors also thank Coordenação de Aperfeiçoamento de Pessoal de Nível Superior (CAPES) for their financial support.

-
- [1] C. Pethick and H. Smith, *Bose-Einstein Condensation in Dilute Gases*, 2nd ed. (Cambridge University Press, New York, 2008).
 - [2] L.P. Pitaevskii and S. Stringari, *Bose-Einstein Condensation and Superfluidity*, 2nd ed. (Oxford University Press, New York, 2016).
 - [3] I. Bloch, J. Dalibard, and W. Zwerger, Many-body physics with ultracold gases, *Rev. Mod. Phys.* **80**, 885 (2008).
 - [4] E. R. Elliott, M. C. Krutzik, J. R. Williams, R. J. Thompson, and D. C. Aveline, NASA’s cold atom lab (CAL): System development and ground test status, *npj Microgr.* **4**, 16 (2018).
 - [5] N. Lundblad, R. A. Carollo, C. Lannert, M. J. Gold, X. Jiang, D. Paseltiner, N. Sergay, and D. C. Aveline, Shell potentials for microgravity Bose-Einstein condensates, *npj Microgr.* **5**, 30 (2019).
 - [6] S. J. Bereta, L. Madeira, V. S. Bagnato, and M. A. Caracanhas, Bose-Einstein condensation in spherically symmetric traps, *Am. J. Phys.* **87**, 924 (2019).
 - [7] A. Tononi and L. Salasnich, Bose-Einstein Condensation on the Surface of a Sphere, *Phys. Rev. Lett.* **123**, 160403 (2019).
 - [8] N. E. Guenther, P. Massignan, and A. L. Fetter, Quantized superfluid vortex dynamics on cylindrical surfaces and planar annuli, *Phys. Rev. A* **96**, 063608 (2017).
 - [9] P. Massignan and A. L. Fetter, Superfluid vortex dynamics on planar sectors and cones, *Phys. Rev. A* **99**, 063602 (2019).
 - [10] H. Lamb, *Hydrodynamics*, 6th ed. (Dover Publications, New York, 1945).
 - [11] V. A. Bogomolov, Dynamics of vorticity at a sphere, *Fluid Dyn.* **12**, 863 (1977).

- [12] Y. Kimura and H. Okamoto, Vortex motion on a sphere, *J. Phys. Soc. Jpn.* **56**, 4203 (1987).
- [13] Y. Kimura and H. Okamoto, Vortex motion on surfaces with constant curvature, *Proc. R. Soc. Lond. A* **455**, 245 (1999).
- [14] P. K. Newton, *The N-Vortex Problem* (Springer-Verlag, New York, 2001).
- [15] A. M. Turner, V. Vitelli, and D. R. Nelson, Vortices on curved surfaces, *Rev. Mod. Phys.* **82**, 1301 (2010).
- [16] E. Butkov, *Mathematical Physics* (Addison-Wesley, New York, 1973).
- [17] See Supplemental Material at <http://link.aps.org/supplemental/10.1103/PhysRevA.103.053306> for complete simulations of (1) of the dynamics of two vortex-dipoles, (2) a video displaying a simulation of the vortices' orbits for small deviations of their initial positions, and (3) a video of the collision of two asymmetric dipoles (different speeds) with parameters set as in Fig. 4.
- [18] B. P. Anderson, P. C. Haljan, C. E. Wieman, and E. A. Cornell, Vortex Precession in Bose-Einstein Condensates: Observations with Filled and Empty Cores, *Phys. Rev. Lett.* **85**, 2857 (2000).
- [19] T. W. Neely, E. C. Samson, A. S. Bradley, M. J. Davis, and B. P. Anderson, Observation of Vortex Dipoles in an Oblate Bose-Einstein Condensate, *Phys. Rev. Lett.* **104**, 160401 (2010).
- [20] D. V. Freilich, D. M. Bianchi, A. M. Kaufman, T. K. Langin, and D. S. Hall, Real-time dynamics of single vortex lines and vortex dipoles in a Bose-Einstein condensate, *Science* **329**, 1182 (2010).
- [21] K. Padavić, K. Sun, C. Lannert, and S. Vishveshwara, Vortex-antivortex physics in shell-shaped Bose-Einstein condensates, *Phys. Rev. A* **102**, 043305 (2020).
- [22] N. Proukakis, S. Gardiner, M. Davis, and M. Szymańska, *Quantum Gases: Finite Temperature and Non-Equilibrium Dynamics* (Imperial College Press, London, 2013).
- [23] D. C. Aveline, J. R. Williams, E. R. Elliott, C. Dutenhoffer, J. R. Kellogg, J. M. Kohel, N. E. Lay, K. Oudrhiri, R. F. Shotwell, N. Yu, and R. J. Thompson, Observation of Bose-Einstein condensates in an earth orbiting research lab, *Nature (London)* **582**, 193 (2020).
- [24] K. Sun, K. Padavić, F. Yang, S. Vishveshwara, and C. Lannert, Static and dynamic properties of shell-shaped condensates, *Phys. Rev. A* **98**, 013609 (2018).
- [25] J. Zhang and T.-L. Ho, Potential scattering on a spherical surface, *J. Phys. B: At. Mol. Opt. Phys.* **51**, 115301 (2018).
- [26] N. S. Móller, F. E. A. dos Santos, V. S. Bagnato, and A. Pelster, Bose-Einstein condensation on curved manifolds, *New J. Phys.* **22**, 063059 (2020).
- [27] B. M. Garraway and H. Perrin, Recent developments in trapping and manipulation of atoms with adiabatic potentials, *J. Phys. B: At. Mol. Opt. Phys.* **49**, 172001 (2016).
- [28] N. E. Guenther, P. Massignan, and A. L. Fetter, Superfluid vortex dynamics on a torus and other toroidal surfaces of revolution, *Phys. Rev. A* **101**, 053606 (2020).
- [29] A. Tononi, F. Cinti, and L. Salasnich, Quantum Bubbles in Microgravity, *Phys. Rev. Lett.* **125**, 010402 (2020).
- [30] K. Merloti, R. Dubessy, L. Longchambon, A. Perrin, P. E. Pottie, V. Lorent, and H. Perrin, A two-dimensional quantum gas in a magnetic trap, *New J. Phys.* **15**, 033007 (2013).
- [31] Y. Guo, R. Dubessy, M. G. de Herve, A. Kumar, T. Badr, A. Perrin, L. Longchambon, and H. Perrin, Supersonic Rotation of a Superfluid: A Long-Lived Dynamical Ring, *Phys. Rev. Lett.* **124**, 025301 (2020).